Available online at www.sciencedirect.com
SCIENCE DIRECT®
Thin-Walled Structures 43 (2005) 751–771
THIN-WALLED STRUCTURES
www.elsevier.com/locate/tws

Modeling and control of power flow in a double-beam system

J.X. Gao, L. Cheng*

Department of Mechanical Engineering, The Hong Kong Polytechnic University, Hung Hom, Kowloon, Hong Kong, China

Received 9 July 2004; received in revised form 15 October 2004; accepted 10 December 2004

Abstract

The vibrational power flow in a double-beam system is investigated theoretically and experimentally in this paper. A novel large displacement piezoelectric actuator assembly, comprising two curved THUNDER actuators, is used to connect the two beams and provide both passive and active isolation at the same time. A simulation model is proposed to describe the coupled mechanical and electrical properties of the new actuator assembly. Modal expansion approach is used to study the power transmissions between the two beams which are mechanically and electrically coupled via the actuator mounts. The effectiveness of both active and passive isolation has been investigated. The optimal control voltage for each actuator is obtained by minimizing the time-averaged power transmitted into the receiver beam. Results show a significant reduction in vibration power transmission. A correlation between the control effort and the mode shapes to be controlled is shown to exist.

Keywords: THUNDER actuators; Power transmissions; Active and passive isolation; Double-beam system; Control

* Corresponding author. Tel.: +86 852 2766 6769; fax: +86 852 2365 4703.
E-mail address: mmlcheng@polyu.edu.hk (L. Cheng).

0263-8231/$ - see front matter © 2005 Elsevier Ltd. All rights reserved.
doi:10.1016/j.tws.2004.12.003

Nomenclature

$[A]$, $[B]$ matrices containing modal coordinates of the two beams, respectively
E_1 and E_2 Young's modulus of the two beams
$e_1 = (f/V)|_{x=0}$ blocked force of the actuator per unit voltage
$e_2 = (I/x)|_{v=0}$ current per unit displacement
F excitation force applied to the system
f total force generated by the actuator
f_a active force generated by the actuator
f_p passive force generated by the actuator
H superscript which denotes the Hermitian transpose
I electrical current in the actuator
J_1 and J_2 inertia moments of the beams
J_p cost function
K dynamic stiffness of the actuator
M total number of beam modes used in calculations
m_0 mass of the actuator
N total number of actuators
P_a time-averaged power flow into the actuators
P_s time-averaged power flow into the receiver beam
P_0 time-averaged power input to the source beam
V electrical voltage applied to the actuator
$y_1(x)$,$y_2(x)$ transverse displacements of the source and receiver beams, respectively
$y_1(x)^*$,$y_2(x)^*$ complex conjugate of $y_1(x)$,$y_2(x)$, respectively
$\Re = (I/V)|_{x=0}$ electrical admittance of the actuator
ρ_1 and ρ_2 mass densities of the two beams, respectively
η loss factor of the actuator
$\delta(x)$ Dirac delta function
ω angular frequency of excitation force
$[\psi(x)]$,$[\phi(x)]$ matrices of eigenfunctions of the two beams, respectively
ω_m,Ω_m natural frequencies of the two beams, respectively

1. Introduction

Conventional methods for controlling vibration transmission between structures usually use passive isolators with appropriate stiffness and damping. One of the major problems associated with the passive isolation is the loss of performance at low frequencies. In recent years, a considerable amount of work has been carried out on the application of active control to enhance the performance of passive isolations, or more specifically to improve the low frequency performance. A good summary can be found in Fuller et al. [1] and Hansen and Snyder [2], in which various analytic models, control strategies and the characteristics of different types of actuators were presented.

Power flow has been widely used as a parameter to quantify the vibration transmission between structures. Early examples were presented by Goyder and White [3,4]. Subsequently, the method has been used by many others. Jenkins et al. [5] used a secondary force in parallel with an existing passive mount to investigate the efficiency of a one-degree-of-freedom isolation mount. Koh and White [6,7] investigated both force and moment excitations in the power transmission into beam or plate supporting structures. Gardonio et al. [8,9] used the impedance-mobility matrix to study the vibration power transmission between a rigid mass and beam or plate-like structures using a multi-mount and multi-degree-freedom transmission model. Apart from its use as a parameter to describe the vibration transmission, the concept of power flow has also been used as an objective function in optimal control analysis, e.g. Pan and Hansen [10,11] applied this strategy to reduce the vibration transmission between a rigid body and a simply-supported beam.

From a different perspective, actuators, which provide active control action in an active control system, play a crucial role. The use of various types of actuators in active control applications has been reported in the literature, e.g. electromagnetic actuators, hydraulic system, piezoelectric wafers and shape memory alloy (SMA). Electrodynamic actuators and hydraulic system are widely used in the design of isolating systems [1,2,10,11]. However, they usually suffer from large size and heavy weight. Using piezoelectric stacks as actuators, Scribner et al. [12] applied feedback control to achieve narrow-band active isolation. Conventional piezoelectric actuators, however, can only provide very small displacement, whilst low frequency vibrations often involving larger deformation. Although SMA actuators are able to generate a much larger deformation, the dynamic response is much too slow, limiting their use to ultra-low frequency range. Due to the aforementioned drawbacks, there has been a persistent interest in seeking high performance actuators suitable for active control [13–15]. Among various candidates, THUNDER [14] (thin layer composite unimorph ferroelectric driver) exhibits much larger displacement than other conventional piezoelectric actuators. Together with its inherent flexibility, this type of actuators may be a good candidate in the application of active vibration isolation. An attempt has been made to use THUNDERs in the design of automotive seats [16]. Marouze and Cheng [17] reported a feasibility study of active vibration isolation using THUNDERs in a one-degree freedom system. Although these work pointed to the promising feature of the concept, they also demonstrated the practical difficulty of using a THUNDER directly as an active mount due to its curved shape and harsh requirement in its installation. Furthermore, the use of THUNDER actuators in flexible structures still needs further investigation.

In this paper, a novel actuator assembly, comprising two THUNDERs in clamshell configuration, is used as active mount to control the power flow between two vibrating beams. A model that has been previously developed to describe the electromechanical properties of the actuator assembly [18] is further improved to model the whole coupled structure. The effectiveness of both active and passive isolation is assessed. The time-averaged power transmitted into the receiver beam is used as a cost function to be optimized for obtaining the control voltages. Results show that a significant reduction in vibrational power transmission can be achieved using the new actuator assembly over a wide frequency range.

2. Description and modeling of the actuator assembly

2.1. Description of the novel actuator assembly

The presently used THUNDER actuator owes its large displacement range and load capacity to a particular fabrication process [14]. An ultra-high performance hot melt adhesive, LaRC™-SI, is used to bond metal foils to PZT ceramic at an elevated temperature in order to create a pre-stressed condition when cooled down to room temperature. A number of layers, whose coefficients of thermal expansion are different, are bonded, making up the composite laminate and giving the actuator special characteristics. Under an applied voltage, the actuator deforms out of plane, generating much larger displacement than other piezoelectric ceramic actuators. In addition, it can act like a spring due to the flexibility provided by the metal foil. Therefore, this type of actuator may be an ideal candidate for designing an active isolation system, in which both active and passive isolations are needed. A proper installation of the THUNDER is the key factor to fully explore its high displacement and loading capacity [17]. However, its actual installation into a mechanical system is far from simple. The ideal working condition for a THUNDER is to have both ends free, since the vertical displacement at the midpoint of the apex is caused by a change in radius of curvature. It implies that the other end of the THUNDER must be allowed to move freely if one end is constrained, making it very difficult to use in practice. In order to overcome this problem, an actuator assembly is designed in such a way that two THUNDER actuators are put together in a clamshell configuration as shown in Fig. 1. Each end of the THUNDERs is connected to a V-shaped stainless steel clip by small fiber plates as shown in Fig. 1(a). Two small plastic blocks, attached at the midpoints of the THUNDER apex, are used to connect with the structure for displacement and force transmission. Both ends of the actuator assembly can then move freely. Two THUNDERs drive the actuator moving back and forth along the axis vertical to the THUNDER apex when an external voltage is applied as shown in Fig. 1(b). The whole assembly is 12 cm long and 4 cm high, weighting 15.5 g. This actuator assembly possesses similar active and passive properties as a single THUNDER. The passive property of the actuator is not only dependent on the material and the structure of the THUNDER, but also on the properties of steel sheets used in the actuator assembly. The actuator assembly can be conveniently inserted and mounted between the vibrating structures like a spring-type element, such overcoming the existing drawbacks in the actual implementation of THUNDER actuators in a vibration or sound isolation system.

2.2. Modeling of the actuator assembly

A model describing the electromechanical properties of the actuator assembly was developed and validated in our precious work [18]. For the sake of completeness, a brief description of the model is given hereafter. Assuming linearity of elasticity and piezoelectricity, the relationship between the mechanical and electrical characteristics of

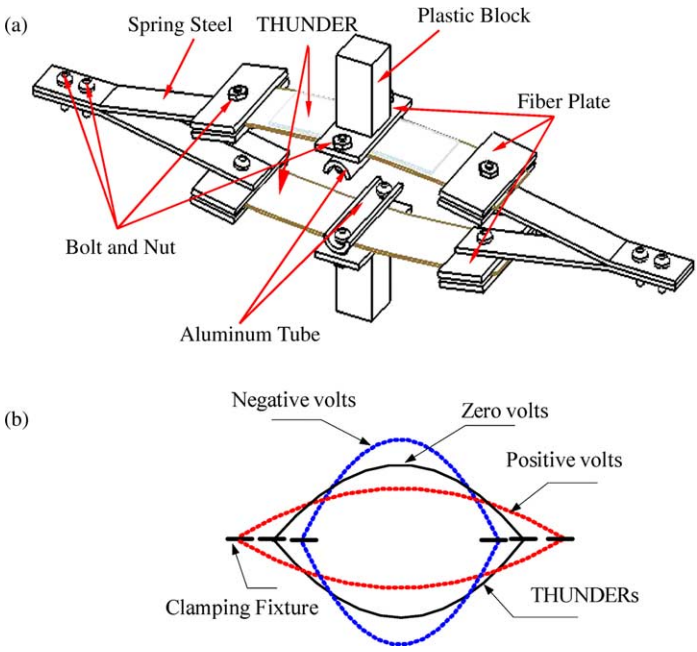

Fig. 1. New actuator assembly: (a) schematic diagram and (b) typical deformations.

the actuator assembly can be expressed as

$$\begin{bmatrix} f \\ I \end{bmatrix} = \begin{bmatrix} K & e_1 \\ e_2 & \Re \end{bmatrix} \begin{bmatrix} x \\ V \end{bmatrix} \tag{1}$$

where f and x are, respectively, the force and the deformation along the vertical direction at the apex of the arc; I and V the electrical current and voltage as shown in Fig. 2. $K=(f/x)|_{v=0}$ is the dynamic stiffness of the actuator with electrical circuit open,

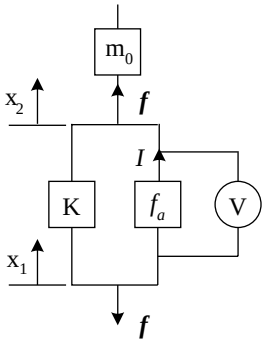

Fig. 2. Schematic model of the actuator.

and $K = K_0(1 + \eta j)$, with η being the internal loss factor. $e_1 = (f/v)|_{x=0}$ is the force per unit voltage when isolator is mechanically blocked. $e_2 = (I/x)|_{V=0}$ is the current per unit displacement with electrical circuit open. $\Re = I/V|_{x=0}$ is the electrical admittance when isolator is mechanically blocked.

It can be seen from Eq. (1) that the force generated by the actuator can be divided into two parts: passive component ($f_p = K\Delta x$) and active component ($f_a = e_I V$). The mass of the actuator itself is included into the model as shown in Fig. 2. Eq. (1) gives the following inter-relationship between different parameters:

$$\text{Without mechanical loading } (f = 0): \ \left.\frac{x}{V}\right|_{f=0} = -\frac{e_1}{K}; \tag{2a}$$

$$\text{With actuator mechanically blocked } (x = 0): \ \left.\frac{f}{V}\right|_{x=0} = -e_1 \tag{2b}$$

These two qualities can be measured under their corresponding conditions. Knowing the electrical admittance of the actuator $\Re|_{x=0}$, other parameters involved in Eq. (1) can be determined. Detailed descriptions of the test set-up and results can be found in [18]. It was noticed that both the free displacement and the blocked force of the actuator were frequency-dependent. The structural characteristics of the actuator itself also had significant effect on the free displacement and the blocked force. The first five natural frequencies of the actuator assembly are 51, 150, 224, 278 and 354 Hz. As a result, a maximum free displacement is observed at 51 Hz, whilst the maximum blocked force occurring at around 350 Hz (around the fifth natural frequency of the actuator itself). The frequency-dependent characteristics of both blocked force and free displacement are considered in numerical simulations presented in Section 4. Based on the testing results, the blocked force per unit voltage $(f/v)|_{x=0}$ is approximately considered to be a constant of 0.02 N/V at lower frequencies (0–180 Hz), to linearly increase from 180 to 320 Hz and decrease from 320 to 450 Hz, before becoming a constant again of 0.1 N/V at higher frequencies. Typical values of the dynamic stiffness $K = (f/x)|_{V=0}$ are around 10^3 N/m for lower frequencies (0–180 Hz) and about 10^5 N/m for frequencies over 600 Hz. Piecewise representation is used between 180 and 600 Hz to reflect the frequency variation. The loss factor of actuators is set to be 0.05.

3. Governing equations and control strategies

3.1. Equations of motion of the isolating system

The system under investigation is shown in Fig. 3, in which two beams are connected by multiple actuators. The upper beam, subjected to a mechanical excitation $F = F_0\sin(\omega t)$, is referred to as the *source beam*, while the bottom one, receiving transmitted energy from the source beam, being referred to as the *receiver beam*. Energy transmission should be controlled by passive and active effect of the actuators inserted between the two beams. Only vertical motion and force transmissions will be considered. From Eq. (1), the force

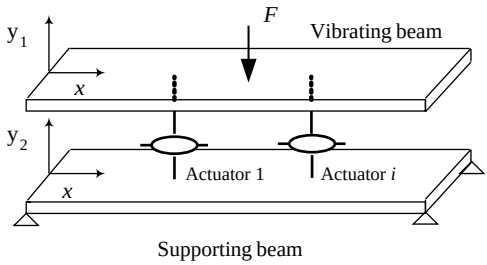

Fig. 3. A generic double-beam system.

generated by the ith actuator, f^i, can be expressed as

$$f^i = K_i[y_1(x_i) - y_2(x_i)] + e_1 V_i \tag{3}$$

where $y_1(x_i)$,$y_2(x_i)$ are the transverse displacements of the source and receiver beams at the ith mounting point, respectively; V_i the control voltage applied to the ith actuator.

The inertia force induced by the mass of the actuator itself, m_0^i, can be expressed as:

$$f_g^i = -m_0^i[\ddot{y}_1(x_i) - \ddot{y}_2(x_i)] = m_0^i\omega^2[y_1(x_i) - y_2(x_i)] \tag{4}$$

Based on classic beam theory, the governing equations of the system can be expressed as

$$\begin{aligned} E_1J_1\frac{\partial^4 y_1}{\partial x^4} + \rho_1 h_1\frac{\partial^2 y_1}{\partial t^2} &= F\delta(x - x_f) - \sum_{i=1}^{N} f^i\delta(x - x_i) + \sum_{i=1}^{N} f_g^i\delta(x - x_i) \\ E_2J_2\frac{\partial^4 y_2}{\partial x^4} + \rho_2 h_2\frac{\partial^2 y_2}{\partial t^2} &= \sum_{i=1}^{N} f^i\delta(x - x_i) - \sum_{i=1}^{N} f_g^i\delta(x - x_i) \end{aligned} \tag{5}$$

where, E_1,ρ_1,J_1 and E_2,ρ_2,J_2 are the elastic modulus, mass density and the inertia moment of the two beams, respectively; $\delta(x-x_i)$ the Dirac delta function and N the total number of actuators.

The transverse displacement of each beam can be expressed using the eigenfunction expansion theorem as

$$\begin{aligned} y_1(x,t) &= \sum_{m=1}^{M} A_m\psi_m(x)\sin(\omega t) = [\psi(x)][A]\sin(\omega t) \\ y_2(x,t) &= \sum_{m=1}^{M} B_m\phi_m(x)\sin(\omega t) = [\phi(x)][B]\sin(\omega t) \end{aligned} \tag{6}$$

with

$$[\psi(x)] = [\psi_1(x), \psi_2(x), \ldots, \psi_M(x)], \quad [\phi(x,y)] = [\phi_1(x), \phi_2(x), \ldots, \phi_M(x)]$$

$$[A] = [A_1, A_2, \ldots, A_M]^{\mathrm{T}}, \quad [B] = [B_1, B_2, \ldots, B_M]^{\mathrm{T}}$$

where $\psi_m(x)$, $\phi_m(x)$ are the mth eigenfunctions of the beams.

Applying orthogonal properties of the eigenfunctions to Eq. (5) yields

$$\begin{aligned}
\Lambda_m\left[\omega_m^2(1+j\eta_m)-\omega^2\right]A_m &= \int_0^a \left\{F_0\delta(x-x_f) - \sum_{i=1}^{N}[f^i - f_g^i]\delta(x-x_i)\right\}\psi_m(x)\mathrm{d}x \\
&= F_0\psi_m(x_f) - \sum_{i=1}^{N}[f^i(x_i) - f_g^i(x_i)]\psi_m(x_i) \\
\Gamma_m[\Omega_m^2(1+j\varsigma_m)-\omega^2]B_m &= \int_0^b \sum_{i=1}^{N}[f^i - f_g^i]\delta(x-x_i)\phi_m(x)\mathrm{d}x \\
&= \sum_{i=1}^{N}[f^i(x_i) - f_g^i(x_i)]\phi_m(x_i)
\end{aligned} \tag{7}$$

where, ω is the excitation frequency; ω_m, Ω_m are the natural frequencies of beams which can be readily obtained for given boundary conditions.

Rearranging Eq. (7) in matrix form gives

$$\begin{aligned}
[M_1][A] &= F_0[\psi(x_f)]^{\mathrm{T}} + \sum_{i=1}^{N}[m_0^i\omega^2 - K_i]\{[\psi(x_i)]^{\mathrm{T}}[\psi(x_i)][A] - [\psi(x_i)]^{\mathrm{T}}[\phi(x_i)][B]\} \\
&\quad - \sum_{i=1}^{N} e_1 V_i[\psi(x_i)]^{\mathrm{T}} \\
[M_2][B] &= -\sum_{i=1}^{N}[m_0^i\omega^2 - K_i]\{[\phi(x_i)]^{\mathrm{T}}[\psi(x_i)][A] - [\phi(x_i)]^{\mathrm{T}}[\phi(x_i)][B]\} \\
&\quad + \sum_{i=1}^{N} e_1 V_i[\phi(x_i)]^{\mathrm{T}}
\end{aligned} \tag{8}$$

which can be further arranged as

$$\begin{bmatrix}[C_{11}] & [C_{12}] \\ [C_{21}] & [C_{22}]\end{bmatrix}\begin{bmatrix}[A] \\ [B]\end{bmatrix} = \begin{bmatrix}[F_{11}] + [F_{12}] \\ [F_{22}]\end{bmatrix} \tag{9}$$

where

$$[C_{11}] = [M_1] + \sum_{i=1}^{N}[K_i - m_0^i\omega^2][\psi(x_i)]^{\mathrm{T}}[\psi(x_i)],$$

$$[C_{12}] = -\sum_{i=1}^{N}[K_i - m_0^i\omega^2][\psi(x_i)]^{\mathrm{T}}[\phi(x_i)]$$

$$[C_{21}] = -\sum_{i=1}^{N}[K_i - m_0^i\omega^2][\phi(x_i)]^{\mathrm{T}}[\psi(x_i)],$$

$$[C_{22}] = [M_2] + \sum_{i=1}^{N}[K_i - m_0^i\omega^2][\phi(x_i)]^{\mathrm{T}}[\phi(x_i)]$$

$$[F_{11}] = F_0[\psi(x_f)]^{\mathrm{T}}, \quad [F_{12}] = -\sum_{i=1}^{N} e_1 V_i[\psi(x_i)]^{\mathrm{T}}, \quad [F_{22}] = \sum_{i=1}^{N} e_1 V_i[\phi(x_i)]^{\mathrm{T}}$$

3.2. Vibration transmissions and optimal control

The time-averaged power input to the source beam by a point harmonic force can be calculated by [8–11]

$$P_0 = \frac{1}{2}\mathrm{Re}\{F\dot{y}_1(x_f)^*\} = -\frac{1}{2}\mathrm{Re}\{j\omega F y_1(x_f)^*\} = \frac{1}{4}\{F^*\dot{y}_1(x_f) + \dot{y}_1(x_f)^* F\} \tag{10}$$

where $y_1(x_f)$ is the displacement of the beam at the excitation point and $y_1(x_f)^*$ is the complex conjugate of $y_1(x_f)$.

The power flow into the actuators is estimated using

$$P_{\mathrm{a}} = -\frac{1}{2}\sum_{i=1}^{N}\mathrm{Re}\{j\omega f_i y_1(x_i)^*\} \tag{11}$$

The total power flow into the receiver beam is the sum of the power flows through all actuators

$$P_{\mathrm{s}} = \frac{1}{2}\sum_{i=1}^{N}\mathrm{Re}\{f_i\dot{y}_2(x_i)^*\} = \frac{j\omega}{4}\sum_{i}^{N}\{f_i^* y_2(x_i) - y_2(x_i)^* f_i\} \tag{12}$$

where f_i is the force generated by the actuator; $y_1(x_{\mathrm{i}})^*$, $y_2(x_{\mathrm{i}})^*$ the complex conjugate of the displacements at the connecting points between the actuators and beams. The difference between P_{a} and P_{s} is the energy dissipation by the actuators.

Solving Eq. (9) yields

$$\begin{bmatrix}[A]\\ [B]\end{bmatrix} = \begin{bmatrix}[D_{11}] & [D_{12}]\\ [D_{21}] & [D_{22}]\end{bmatrix}\begin{bmatrix}[F_{11}] + [F_{12}]\\ [F_{22}]\end{bmatrix} \tag{13}$$

where

$$\begin{bmatrix} [D_{11}] & [D_{12}] \\ [D_{21}] & [D_{22}] \end{bmatrix} = \begin{bmatrix} [C_{11}] & [C_{12}] \\ [C_{21}] & [C_{22}] \end{bmatrix}^{-1}$$

Substituting (13) into Eqs. (6) and (3), the displacement of the beams can be calculated as

$$\begin{aligned} y_1(x_i) &= [\psi(x_i)][A] = [\psi(x_i)][D_{11}]\{[F_{11}] + [F_{12}]\} + [\psi(x_i)][D_{12}][F_{22}] = b_{01}^i + [b_1^i][V] \\ y_2(x_i) &= [\phi(x_i)][B] = [\phi(x_i)][D_{21}]\{[F_{11}] + [F_{12}]\} \\ &\quad + [\phi(x_i)][D_{22}][F_{22}] = b_{02}^i + [b_2^i][V] \end{aligned} \tag{14}$$

where $[V] = [V_1, V_2, \ldots, V_N]^{\mathrm{T}}$ is the control voltage matrix applied to the actuators. $b_{01}^i = F_0[\psi(x_i)][D_{11}][\psi(x_f)]^{\mathrm{T}}$, $b_{02}^i = F_0[\phi(x_i)][D_{21}][\psi(x_0)]^{\mathrm{T}}$, $[b_1^i] = [b_{11}, b_{12}, \ldots, b_{1i}, \ldots, b_{1N}]$ and $[b_2^i] = [b_{21}, b_{22}, \ldots, b_{2i}, \ldots, b_{2N}]$, where $b_{1i} = e_i\{[\psi(x_i)][D_{12}][\phi(x_i)]^{\mathrm{T}} - [\psi(x_i)][D_{11}][\psi(x_i)]^{\mathrm{T}}\}$, and $b_{2i} = e_i\{[\phi(x_i)][D_{22}][\phi(x_i)]^{\mathrm{T}} - [\phi(x_i)][D_{21}][\psi(x_i)]^{\mathrm{T}}\}$

The forces generated by the actuators can then be obtained as

$$f_i = K_i[y_1(x_i) - y_2(x_i)] + e_1 V_i = [c_{0i}] + [c_i][V] \tag{15}$$

$$c_{0i} = K[b_{01}^i - b_{02}^i], \quad c_i = K\{[b_1^i] - [b_2^i]\} + b_{ei}, \quad b_{ei} = [0, 0, \ldots, e_i, \ldots, 0]$$

It can be seen that both the displacement of the beams and the force produced by the actuators are linear functions of the control voltage. The purpose of the active control is to minimize the vibration transmission to the beam. Therefore, the total power flow into the receiver beam is chosen as the cost function. Substituting Eqs. (14) and (15) into (12), the cost function can be expressed as the following quadratic function of control voltage matrix $[V]$

$$J_{\mathrm{p}} = \frac{j\omega}{4}\{[V]^{\mathrm{H}}[a][V] + [V]^{\mathrm{H}}[b] + [b]^{\mathrm{H}}[V] + [c]\} \tag{16}$$

where,

$$[a] = \sum_{i=1}^{I}\{[c_i]^{\mathrm{H}}[b_2^i] - [b_2^i]^{\mathrm{H}}[c_i]\}, \quad [b] = \sum_{i=1}^{I}\{[c_i]^{\mathrm{H}}[b_{02}^i] - [b_2^i]^{\mathrm{H}}[c_{0i}]\}$$

$$[c] = \sum_{i=1}^{I}\{[c_{0i}]^{\mathrm{H}}[b_{02}^i] - [b_{02}^i]^{\mathrm{H}}[c_{0i}]\}$$

In the above equations, the superscript H denotes the Hermitian transpose.

The optimal control voltages for actuators can then be obtained by minimizing the cost function, which takes the following form

$$[V] = -[a]^{-1}[c] \tag{17}$$

leading to a minimum value of the cost function:

$$J_{\text{p min}} = [c] - [b]^{\text{H}}[a][b] \tag{18}$$

4. Examples and theoretical and experimental discussions

In the following example, the whole system is composed of two cantilever beams which are connected by several actuators. First, the case of one actuator between the two beams as shown in Fig. 4 is studied numerically and experimentally. The two cantilever beams are all made of aluminum with a density $\rho = 2700\ \text{kg/m}^3$, an elasticity modulus $E = 7.2 \times 10^{10}\ \text{N/m}^2$ and Poisson's ratio $\upsilon = 0.3$. The lengths of the two beams are $a = 0.25$ m, $b = 0.20$ m, respectively, both having the same thickness $h = 2$ mm and width $d = 40$ mm. The modal loss factors of both beams are 0.01 for all modes. A vertical exciting force is applied at the source beam. Calculations show that numerical values are accurate enough within the frequency range of interest as the number of beam modes is $M = 10$. The mechanical and electrical parameters of actuators discussed in Section 2 are used in the simulations.

In parallel, experiments using the same configuration described above are carried out to validate the simulation model. Experimental set-up is shown in Fig. 5. One end of each beam is clamped on a rigid steel frame. A shaker (B&K Mini Shaker 4810) exerts a driving force, which is measured by a force transducer (B&K 8200), on the source beam. Accelerometers (B&K type) are used to measure the responses of the beams. The control signal applied to the actuator is amplified by a Piezo Driver/Amplifier (TReK PZD 700). The measured data are then processed using a Multi-channel Signal Analyzer (B&K type 3550).

The first five resonance frequencies of each uncoupled beam are calculated and tabulated in Table 1. Table 2 lists the first ten resonance frequencies of the coupled beam system obtained by calculation using Eq. (9) by removing the right hand side terms. The table shows the influence of the actuator location and the mass of the actuator. When comparing Tables 1 and 2, it can be seen that when the mass of the actuator is neglected, the coupled natural frequencies of the system are actually very close to these of each individual beam before they are coupled together. The stiffness of the actuator slightly

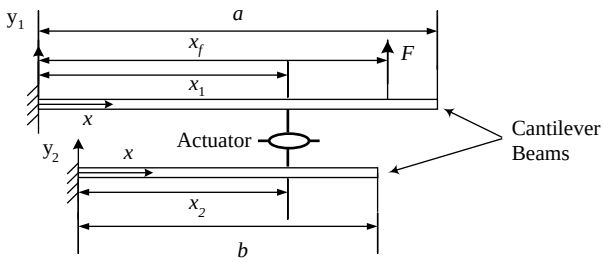

Fig. 4. Two cantilever beams connected by an actuator.

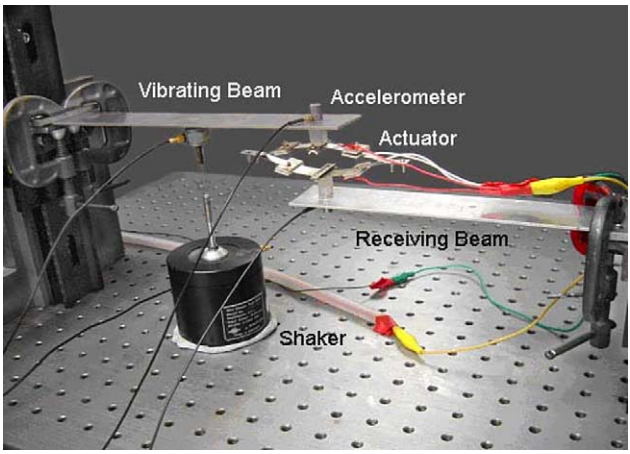

Fig. 5. Experimental set-up.

increases the values of the natural frequencies with the first mode being most affected, implying a weak coupling between the beams in the present case. Further consideration of the actuator mass reduces the resonance frequencies, especially for some of the higher order modes. It can also been found from Table 2 that the location of the actuator has a large effect on the modal frequencies of the coupled system, especially when the mass of the actuator is considered. For example, the fifth and sixth modal frequencies (468.2 and 731.8 Hz), and ninth and tenth modal frequencies (1517.4 and 2370.9 Hz) of the coupled beams are seldom affected by the presence of the actuator when the actuator located at $x_1=0.5a$, $x_2=0.5b$ because the connecting point is located near the modal nodal points of the beams. Similar results are observed when $x_1=0.8a$, $x_2=0.8b$ for the third and fourth modes. When the actuator is located at $x_1=0.9a$, $x_2=0.9b$, however, the actuator has

Table 1
Calculated resonance frequencies of two uncoupled beams (Hz)

The source beam	The receiver beam
26.7, 167.3, 468.3, 917.9, 1517.4	41.7, 261.4, 731.8, 1434.2, 2370.9

Table 2
Calculated resonance frequencies of the coupled system (Hz)

Locations of the actuator	The mass of the actuator is not considered ($m_0=0$)	The mass of the actuator is considered ($m_0=15.5$ g)
$x_1=0.5a$	28.6, 169.0, 468.2, 918.2, 1517.4	27.4, 137.1, 468.2, 827.0, 1517.4
$x_2=0.5b$	43.7, 262.8, 731.8, 1434.5, 2370.9	40.7, 231.0, 731.6, 1317.5, 2370.9
$x_1=0.8a$	31.7, 167.3, 468.5, 918.2, 1517.5	28.8, 167.1, 449.4, 852.9, 1490.6
$x_2=0.8b$	52.7, 261.4, 731.9, 1434.4, 2371.0	38.9, 261.0, 691.3, 1295.7, 2261.7
$x_1=0.9a$	32.3, 168.3, 468.4, 917.9 1517.4	29.2, 159.0, 464.8, 917.6, 1498.4
$x_2=0.9b$	57.1, 262.1, 731.8, 1434.2, 2370.9	38.3, 248.3, 724.8, 1413.2, 2335.6

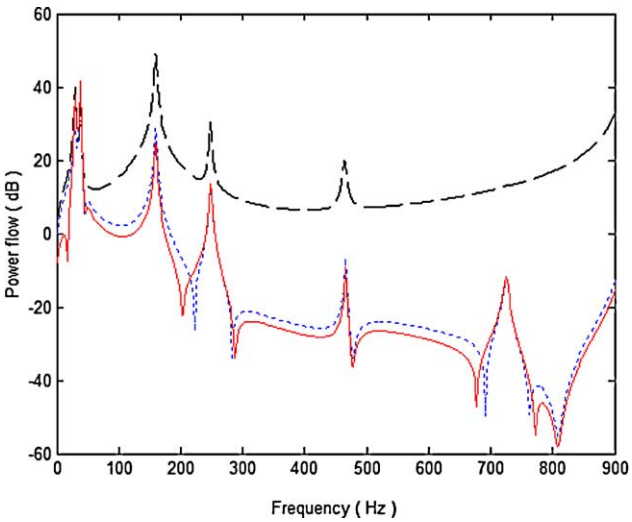

Fig. 6. Time-averaged power flows (dB ref: 10^{-5} W) under passive control when an unit exciting force is applied at $x_f = 0.5a$, and a actuator is located at $x_1 = 0.9a$, $x_2 = 0.9b$: (– – –) into the source beam; (- - -) into the actuator; (—) into the receiver beam.

obvious influence on a large number of modal frequencies since the connecting point is far from any modal nodal points of the beams.

The passive effect of the actuator on the vibration transmission is first discussed. An exciting force of 1 N is applied at the middle of the source beam and the actuator is located at $x_1 = 0.9a, x_2 = 0.9b$ with no voltage applied to the actuator. Fig. 6 shows the calculated time-averaged power flow into three different components: the power input to the source beam from the external force at the exciting point; the power flow into the actuator and the power into the receiver beam through the actuator. It can be seen that all three curves have common peaks within 0–500 Hz, which correspond to the resonances of the coupled system. The commonality among all these resonances is that each mode involves significant motion of the source beam. Exception occurs for 724.8 Hz mode, at which no peak is observed for the source beam. Further investigation shows that this mode is dominated by the motion of the receiver beam. The general tendency of the curves indicates a more significant power transmission into the receiver beam at low frequencies than high frequencies. It is also worth mentioning that the difference between the power flow into the actuator and the one into the receiver beam is small, pointing to the fact that the energy dissipated by the actuator itself is small due to the trivial damping value used in the model.

The above configuration is also used for model validation. Fig. 7(a) and (b) show comparisons between numerical and experimental results in terms of power flows into the source beam and the receiver beam, respectively. In the experimental tests, a harmonic excitation force was applied at the middle of the source beam as shown in Fig. 5 with the exciting frequency gradually increased from 5 to 300 Hz. It can be seen that there is an agreement between the two sets of data. More specifically, the experimental and numerical results match very well in the range of 0–150 Hz, while more obvious deviation appears

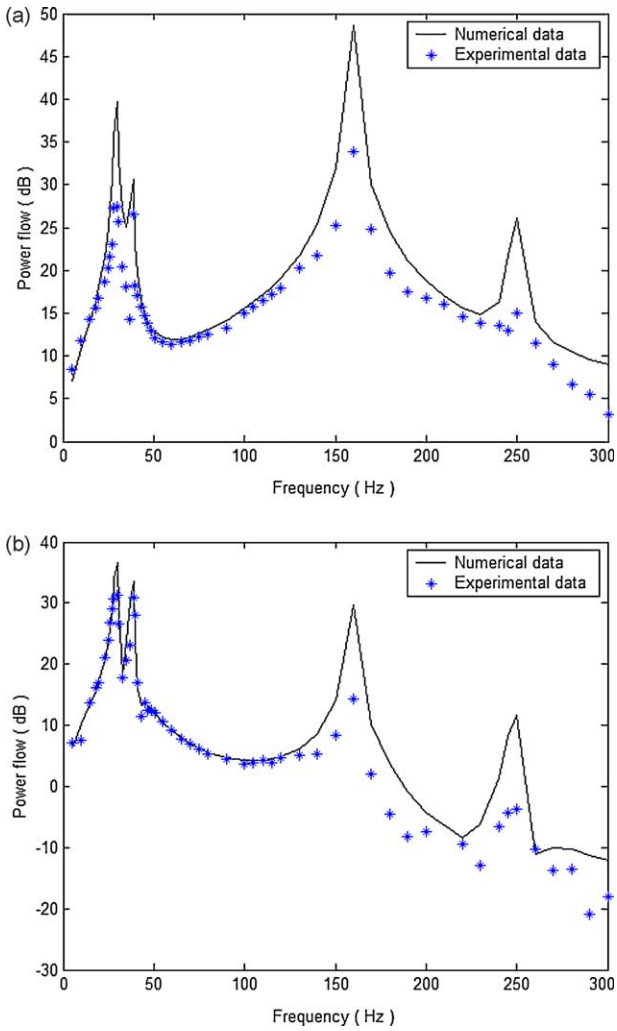

Fig. 7. Comparison between numerical and experimental power flows (dB re: 10^{-5} W) when only passive effect is considered: (a) results for the source beam and (b) results for the receiver beam.

when frequency increases. This observation is consistent with that obtained in [18], which also showed a more obvious discrepancy between simulation and experiments above 200 Hz. The simple model used for the actuator assembly, apparently suitable for low frequency analysis, is questionable when entering to the range of second and third modes of the actuator itself. Generally speaking however, the simulation model presented in this paper seems to correctly simulate the dynamic behavior of the whole system with the passive effect of the actuators taken into account.

The combined active and passive effect of the actuator assembly on the vibration isolation is discussed hereafter. Fig. 8(a) shows the numerical time-averaged power input

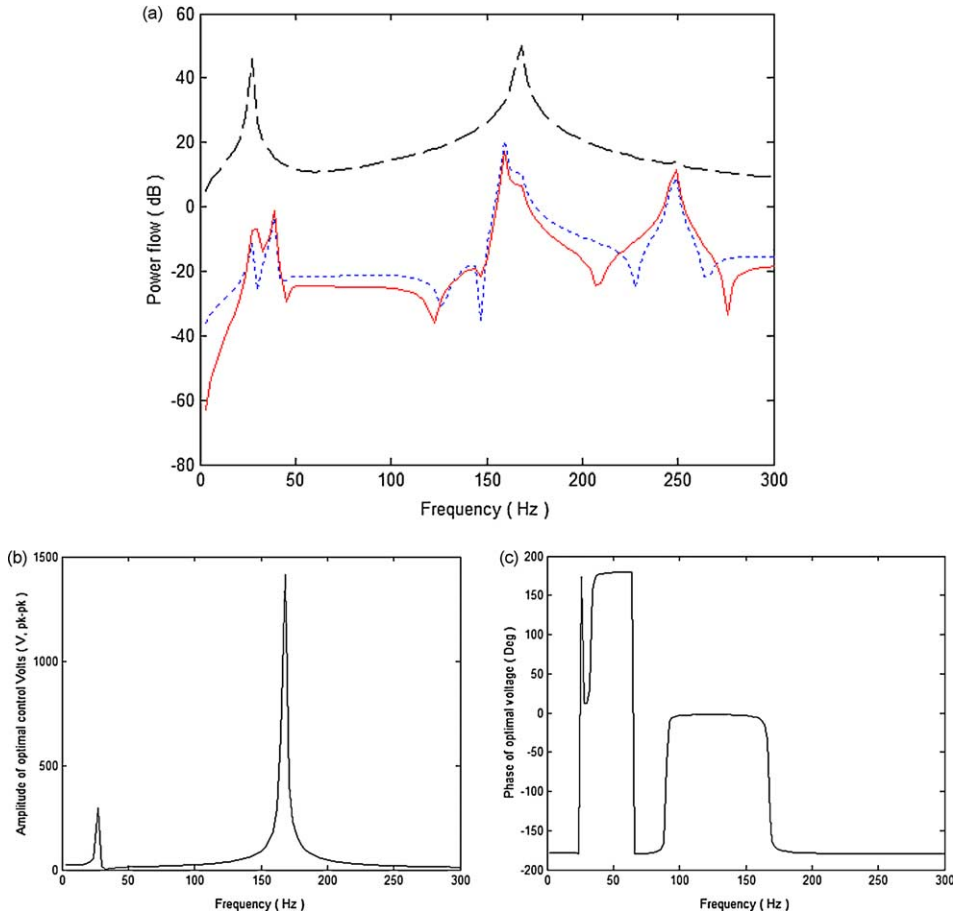

Fig. 8. (a) Calculated time-averaged power flow (dB ref: 10^{-5} W) under optimal active control: (– – –) into the source beam; (- - -) into the actuator; (—) into the receiver beam when an exciting force of 1 N is applied at $x_f = 0.5a$ and a actuator is located at $x_1 = 0.9a$, $x_2 = 0.9b$; (b) amplitude of the optimal control voltage; and (c) phase of the optimal control voltage.

to the source beam, to the actuator and to the receiver beam within lower frequency (0–300 Hz), when an active control voltage is applied to the actuator. It can be seen that although the action of the actuator alters the power input to the source beam, the overall level remains comparable with the passive case as shown in Fig. 6. The power transmitted into the receiver beam, however, is significantly reduced by the active effect of the actuator within this frequency range. When comparing with the passive control case shown in Fig. 6, the reduction is particularly significant before 150 Hz, covering the first two modes of the system, and to a lesser extent above this frequency. It is relevant to investigate the control effort needed to achieve the aforementioned control performance. Fig. 8(b) and (c) give the amplitude and the phase of the optimal control voltage versus frequencies, respectively. It can be seen that the required control voltage largely depends on

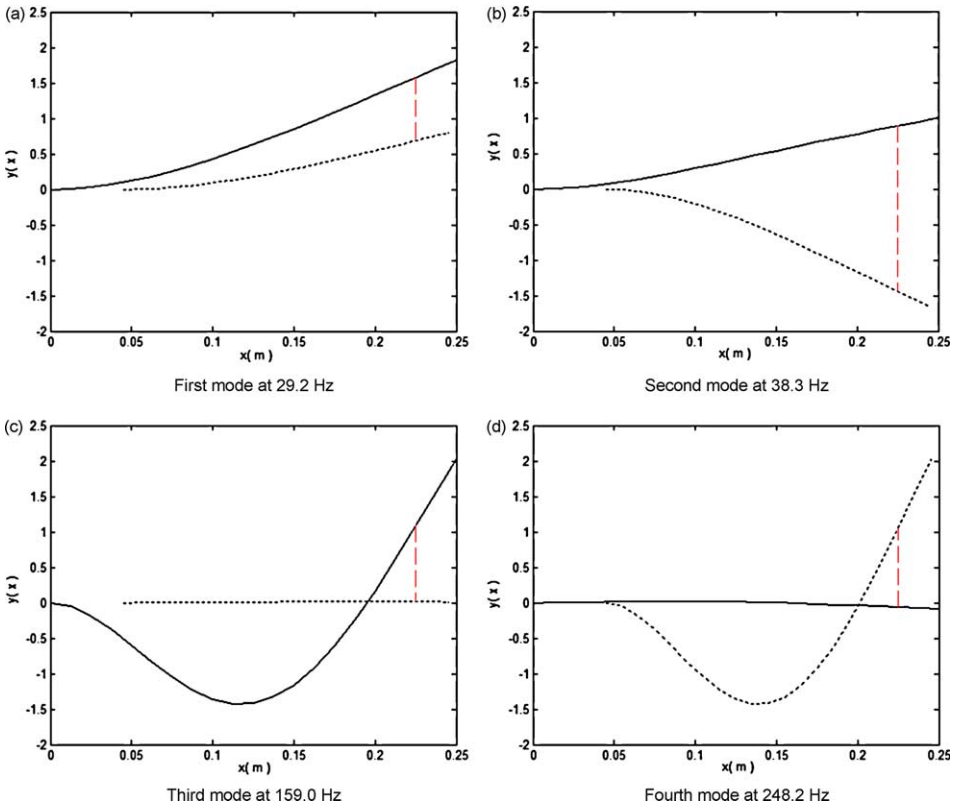

Fig. 9. The first four mode shapes of two coupled beams: (—) source beam; (- - -) receiver beam. An actuator is located at $x_1 = 0.9a$, $x_2 = 0.9b$.

the frequency and the modes to be controlled. Within the frequency of interest in which the first four structural modes are involved, the first mode (29.2 Hz) and the third mode (159 Hz) require relatively high voltage input. This phenomenon can be explained by examining Fig. 9, which shows the first four mode shapes of the coupled system. It is obvious that the third mode is dominated by the motion of the source beam. The receiver beam, however, undergoes negligible motion compared to the source beam. As a result, the low mobility of the receiver beam requires high actuation level. This observation also applies to the first mode to a lesser degree, in which the receiver beam has relatively lower mobility compared to the second and fourth modes. At the same time, Fig. 9(b) and (d) show another commonality of these two modes. In fact, both beams move in anti-phase. Considering the actual effect of the actuators, this anti-phase motion between the two beams makes the control easier. The coupling characteristics of two coupled structures have been investigated in details in [19,20]. The concept put forward in those papers can help classify modes for controllability assessment. For the present configuration, modes of the double-beam system can be divided into three categories: (1) the modes dominated by source beam, in which the source beam undergoes much larger motion than the receiver

beam such as mode 3; (2) the modes dominated by the receiver beam such as mode 4; and (3) well-coupled modes which involve significant motions from both beams such as modes 1 and 2. From the control point of view, it seems that the modes of category (1) are the most difficult ones to be controlled. For the well-coupled modes, the in-phase motion of the beams also requires a higher control effort than the anti-phase motion does.

The modeling of the active effect of actuators is validated using experimental results in Fig. 10. The position of the actuator and the harmonic exciting force remain the same as the previous passive case. During the experimental tests, the amplitude and the phase of the control voltage were adjusted to obtain the minimum vibration on the receiver beam. The control voltage used in the tests is then input to the numerical program to obtain

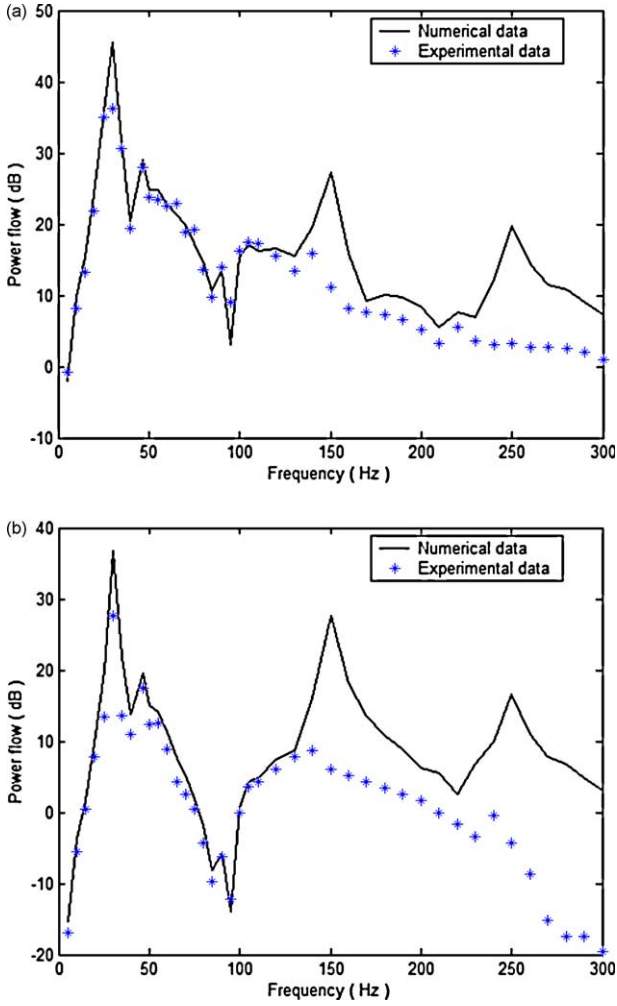

Fig. 10. Comparison between numerical and experimental power flows (dB re: 10^{-5} W) when active control is deployed: (a) power flow into the actuator and (b) power flow into the receiver beam.

the calculated curves. Fig. 10 illustrates again a nice agreement between the experimental and numerical results in the range of frequencies of 0–150 Hz. Comparison between Figs. 10(b) and 7(b) shows that the power transmitted into the receiver beam can be significantly reduced by active control within lower frequency range as predicted by previously performed numerical analysis. The two sets of comparisons between the experimental and numerical results shown in Figs. 7 and 10 demonstrate that the developed model can be effectively used to the simulate of the double-beam system in both passive and active control cases.

Increasing the number of actuators is expected to improve the control performance. Two actuators, located at $x_{11}=0.5a$, $x_{21}=0.5b$ and $x_{12}=0.9a$, $x_{22}=0.9b$, are used between the two cantilevered beams. Fig. 11 shows the total time-averaged power flow into the two actuators and to the two beams, respectively, in passive case with a unit exciting force applied at middle of the source beam. Compared to the case of one actuator, more power is transmitted into the receiver beam in the higher frequency range through the actuators. It can also be noticed that the difference between the power flow into the actuators and that into the receiver beam also becomes larger due to an increase in system damping introduced by the actuators. Comparing Fig. 11 with Fig. 6 also shows a slight increase in resonant frequencies, which is understandable because of an increase in the system stiffness.

Fig. 12(a) shows the calculated total time-averaged power input into the source beam, into the actuators and into the receiver beam when active control is applied. Once again, the vibration power transmitted into the receiver beam can be significantly reduced with the deployment of the active control. Comparing Fig. 12(a) with Fig. 8(a) shows that the system with two actuators has similar active control effectiveness to that with one actuator

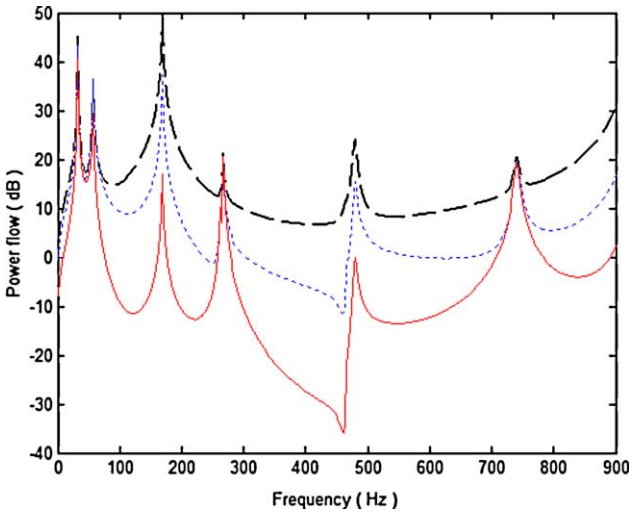

Fig. 11. Total time-averaged power flows (dB ref: 10^{-5} W) with passive action when a unit exciting force is applied at $x_f=0.50$ and two actuators are mounted at $x_{11}=0.5a, x_{21}=0.5b$ and $x_{12}=0.9a, x_{22}=0.9b$, respectively: (– – –) power into source beam; (- - -) total power into the two actuators; (—) total power into the receiver beam.

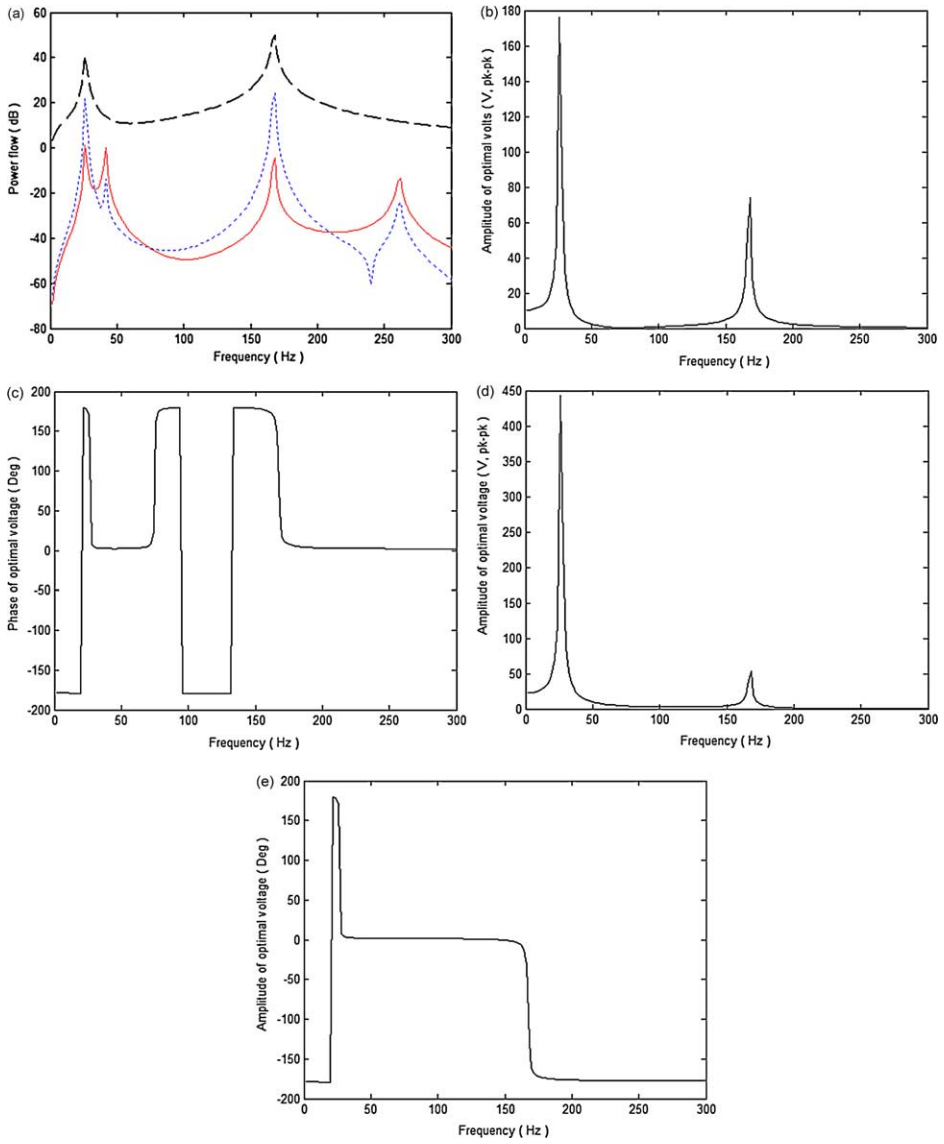

Fig. 12. (a) Total time-averaged power flow (dB ref: 10^{-5} W) under active control: (– – –) into the source beam; (- - -) into the actuators; (—) into the receiver beam, where an exciting force of 1 N is applied at $x_f = 0.5a$ and the two actuators are mounted at $x_{11} = 0.5a$, $x_{21} = 0.5b$ and $x_{12} = 0.9a$, $x_{22} = 0.9b$; (b) and (d) the amplitude of the optimal control voltage for each actuator; (c) and (e) the phase of the optimal control voltage for each actuator.

within 0–50 Hz. However, much better effectiveness (over 20 dB reduction) is achieved within 50–300 Hz. The use of more actuators apparently improves the control performance at higher frequencies, where a single actuator fails. Meanwhile, Fig. 12(b)–(e) show the amplitude and phase of the optimal control voltages required

for each actuator. It demonstrates that the maximum optimal control voltages for the system with two actuators occur at around the first modal frequency, which is different from the case of one actuator. The reason is that mode shapes of the whole system have been altered due to the introduction of the second actuator. At the same time, it can also be noticed that the amplitude of the maximum optimal control voltage is much lower than that required by the system with one actuator. Since there exists a maximum allowable voltage for the THUNDER actuator, using more actuators proves beneficial in respecting this limit and increasing the control performance at the same time.

5. Conclusions

A novel actuator assembly is used to actively control the vibration transmission between two beams. Providing both passive and active action, the actuator assembly is convenient to use as an active and passive mount. Comparison between experimental and numerical results shows that the developed model can be effectively used in the simulation of the coupled systems in both passive and active cases, especially in the low frequency range. It also reveals that the mass and stiffness of the actuator assembly have large effects on resonant frequencies and responses, especially for the higher frequencies.

The new actuator assembly is shown to provide an excellent performance. The vibrational power transmitted into the receiver beam can be significantly reduced by the active effect of the actuators within lower frequency range. Generally speaking, higher control voltage is needed to control modes dominated by the motion of the source beam, in which the receiver beam only undergoes small motion. For strongly coupled modes, the one involving an in-phase motion of the two beams also requires higher control effort. Increasing the number of actuators can further improve the control performance while lowing down the actuation level required.

Acknowledgements

The work described in this paper was fully supported by a grant from Research Grants Council of Hong Kong Special Administrative Region, China (Project No. PolyU 5155/01E).

References

[1] Fuller CR, Elliott SJ, Nelson PA. Active control of vibration. New York: Academic Press; 1996.
[2] Hansen CH, Snyder SD. Active control of noise and vibration. London: E&FN SPON; 1997.
[3] Goyder HGD, White RG. Vibrational power flow from machines into built-up structures, part 1: introduction and approximate analyses of beam and plate-like foundation. J Sound Vib 1980;68:59–75.
[4] Goyder HGD, White RG. Vibrational power flow from machines into built-up structures, part 3: power flow through isolation system. J Sound Vib 1980;68:97–117.
[5] Jenkins MD, Nelson PA, Pinnington RJ, Elliott SJ. Active isolation of periodic machinery vibration. J Sound Vib 1993;166:117–40.

[6] Koh YK, White RG. Analysis and control of vibration power transmission to machinery supporting structures subjected to a multi-excitation system, part 1: driving point mobility matrix of beams and rectangular plates. J Sound Vib 1996;196:469–93.
[7] Koh YK, White RG. Analysis and control of vibration power transmission to machinery supporting structures subjected to a multi-excitation system, part 2: vibration power analysis and control schemes. J Sound Vib 1996;196:495–508.
[8] Gardonio P, Elliott SJ, Pinnington RJ. Active isolation of structural vibration on a multiple-degree-of freedom system, part 1: the dynamics of the system. J Sound Vib 1997;207:61–93.
[9] Gardonio P, Elliott SJ, Pinnington RJ. Active isolation of structural vibration on a multiple-degree-of freedom system, part 2: effectiveness of active control strategies. J Sound Vib 1997;207:85–121.
[10] Pan J, Hansen CH, Pan J. Active isolation of a vibration source from a thin beam using single active mount. J Acoust Soc Am 1993;94:1425–34.
[11] Pan J, Hansen CH. Active control of power flow from a vibrating rigid body to a flexible panel through two active isolators. J Acoust Soc Am 1993;93:1947–53.
[12] Scribner KB, Sievers LA, Von Flotow AH. Active narrow-band vibration of machinery noise from resonant substructures. J Sound Vib 1993;167:17–40.
[13] Garcia-Bonito J, Brennan MJ, Elliott SJ, David A, Pinnington RJ. A novel high-displacement piezoelectric actuator for active vibration control. J Smart Mater Strut 1998;7:31–42.
[14] Copeland BM, Buckley JD, Bryant RG, Fox RL, Hellbaum RF. An ultra-high displacement piezoelectric actuator.: NASA Langley Research Center; 1999 (23681-0001).
[15] Yoon KJ, Shin S, Park HC, Goo NS. Design and manufacture of a lightweight piezoelectric curved actuators. J Smart Mater Strut 2002;11:163–8.
[16] Malowicki M, Leo DJ. Active vibration isolation using an induced strain actuator with application to automotive seat suspensions. Shock Vib 2001;8(5):271–85.
[17] Marouze JP, Cheng L. A feasibility study of active vibration isolation using THUNDER actuators. J Smart Mater Strut 2002;11:854–62.
[18] Gao JX, Cheng L. Modeling of a high performance piezoelectric actuator assembly for active and passive vibration control. J Smart Mater Strut 2004;13:384–92.
[19] Missaoui J, Cheng L, Richard M. Free and forced vibration of a cylindrical shell with a floor partition. J Sound Vib 1996;190:21–40.
[20] Missaoui J, Cheng L. Vibroacoustic analysis of a finite cylindrical shell with a floor partition. J Sound Vib 1999;226:101–23.